Highly Conducting Charge-Transfer Compounds of Tetrathiafulvalene and Transition Metal-"dmit" Complexes

Michèle Bousseau,[1a] Lydie Valade,[1a] Jean-Pierre Legros,[1a] Patrick Cassoux,*[1a] Mary Garbauskas,[1b] and Leonard V. Interrante*[1c]

Contribution from the Laboratoire de Chimie de Coordination du CNRS, Unité n° 8241, liée par convention à l'Université Paul Sabatier, 31400 Toulouse, France, General Electric Corporate R&D, Schenectady, New York 12301, and the Department of Chemistry, Rensselaer Polytechnic Institute, Troy, New York 12180-3590. *Received May 15, 1985*

Abstract: The synthesis, structural characterization, and electrical conductivity studies of the donor-acceptor compounds $TTF[Ni(dmit)_2]_2$, **1**, $TTF[Pd(dmit)_2]_2$, **2**, and $TTF[Pt(dmit)_2]_3$, **3** (TTF = tetrathiafulvalene; H_2dmit = 4,5-dimercapto-1,3-dithiol-2-thione), are described. These compounds were obtained as small needles from the slow interdiffusion of solutions of $(TTF)_3(BF_4)_2$ and $(n\text{-}Bu_4N)[M(dmit)_2]$. Single crystals of **1** have also been obtained by electrosynthesis. Structures of compounds **1** and **3** have been established by X-ray diffraction methods. The monoclinic cell of compound **1**, space group $C2/c$ with $Z = 4$, has cell parameters $a = 46.22$ (3) Å, $b = 3.732$ (2) Å, $c = 22.86$ (1) Å, $\beta = 119.3$ (1)°, and $V = 3439$ Å^3. The structure was refined by a block-diagonal least-squares technique to a final error index of $R_w = 0.097$ with a corresponding $R = 0.117$ for the 154 variables and 1475 unique diffraction data for which $F > 2.5\sigma(F)$. A uniform segregated stacking arrangement of the constituent TTF and $Ni(dmit)_2$ units is observed in which close intermolecular S···S contacts involving sulfur atoms on both types of molecules occur between units in adjacent stacks, leading to a three-dimensional network of closely spaced molecules. The triclinic cell of compound **3**, space group $P\bar{1}$ with $Z = 1$, has cell parameters $a = 6.314$ (5) Å, $b = 11.66$ (2) Å, $c = 16.81$ (3) Å, $\alpha = 84.5$ (1)°, $\beta = 89.6$ (1)°, $\gamma = 81.9$ (1)°, and $V = 1220$ Å^3. The structure has been refined by a block-diagonal least-squares technique to $R_w = 0.101$ with $R = 0.110$ for the 220 variables and 1535 unique diffraction data for which $F > 3\sigma(F)$. This structure consists of $Pt(dmit)_2$ "monomers" and $[Pt(dmit)_2]_2$ "dimers" alternately stacked in columns. The Pt-Pt bond length in a dimer is 2.935 Å. The monomer and dimer columns are arranged in layers, alternating with TTF-containing layers. A number of close intermolecular S···S contacts are observed within the $Pt(dmit)_2$ layers, leading to a two-dimensional network; these are, in turn, coupled to one another in the third dimension by the TTF molecules in the adjacent layers. Crystals of compound **1** exhibit a metallike conductivity temperature dependence down to 4 K, with a conductivity at room temperature of ca. 300 Ω^{-1} cm^{-1} and at 4 K of over 10^5 Ω^{-1} cm^{-1}. Compound **2** exhibits a room-temperature conductivity of ca. 750 Ω^{-1} cm^{-1} and undergoes an apparent metal-to-insulator transition below ca. 220 K. This can be related to structural changes involving three different phases isomorphous with compound **1**. Compound **3** is a semiconductor throughout the 300-100 K temperature range with a room-temperature conductivity of ca. 20 Ω^{-1} cm^{-1}. The conductivity behavior of the three compounds is discussed in the context of their crystal structure and the results of previous work on other molecular metal systems with high molecular connectivity.

Considerable effort has been devoted to the preparation and study of conducting molecular solids and, in particular, the development of "molecular metals" and superconductors.[2-4] The materials of interest in this connection have included both "inorganic" systems, such as $K_2[Pt(CN)_4]Br_{0.3}\cdot 3H_2O$ (KCP),[5,6] $(SN)_x$,[7] and the bis(dithiolene) metal complexes,[8] as well as organic molecular and polymeric systems such as tetrathiafulvalene-tetracyanoquinodimethane (TTF-TCNQ)[3,4] and polyacetylene.[9] An important goal of this research has been the understanding of the role of the intermolecular and intramolecular interactions in determining the electrical properties of this most unusual class of molecular solids.

A characteristic feature of these solids is the propensity for "one-dimensional" (1D) solid-state interactions, owing to the particular combination of the directional character of the frontier orbitals of the constituent molecular units and the chainlike structures in the solid imposed by the molecular and/or crystal structure.[2,4] In the case of the planar transition-metal complexes and organic molecular systems, such as KCP and TTF-TCNQ, the segregated stacking of the constituent planar units leads to highly directional intermolecular d_{z^2} or π orbital interactions and, consequently, a quasi-1D electronic system.

Despite continuing questions regarding the role of sliding charge density waves or other 1D-specific conduction mechanisms in determining the transport properties of such "1D metal" systems,[2] the general emphasis of much of the recent synthetic work in this area has been on the development of systems with enhanced interstack interactions. These efforts are motivated by the desire to avoid the ubiquitous "metal-to-insulator" transition encountered on cooling most 1D metals to low temperatures, arising from the intrinsic instability (Peierls transition) associated with a true 1D metallic system.[10] In the last several years, this approach has been used with considerable success in the generation of molecular systems which retain their metallike characteristics down to very low temperatures and, recently, of the first examples of ambient-pressure molecular superconductors.[11,12]

(1) (a) Laboratoire de Chimie de Coordination. (b) General Electric Corporate R&D. (c) Rensselaer Polytechnic Institute.

(2) (a) Devreese, J. T.; Evrard, R. P.; Van Doren, V. E. "Highly Conducting One-Dimensional Solids"; Plenum Press: New York, 1979. (b) Miller, J. S. "Extended Linear Chain Compounds"; Plenum Press: New York, 1982, Vol. 1, 2; 1983, Vol. 3.

(3) (a) King, R. B. *Adv. Chem. Ser.* **1976**, *No. 150*. (b) Hatfield, N. E. "Molecular Metals"; Plenum Press: New York, 1979; NATO Conference Series—Series VI, Vol. 1. (c) Alcacer, L. "The Physics and Chemistry of Low Dimensional Solids"; Reidel: Dordrecht, 1980; NATO Advanced Study Institutes Series—Series C, Vol. 56.

(4) (a) Proceedings of the International Conference on Low-Dimensional Conductors, Boulder, 1981; *Mol. Cryst. Liq. Cryst.* **1982**, *79*. (b) Proceedings of the Colloque International du CNRS sur la Physique et la Chimie des Mêtaux Synthêtiques et Organiques, Les Arcs, 1982; *J. Phys.* **1983**, *44*. (c) Proceedings of the International Conference on the Physics and Chemistry of Low-Dimensional Synthetic Metals, Abano Terme, 1984; *Mol. Cryst. Liq. Cryst.* **1985**, *120*.

(5) Abbreviations: KCP, $K_2[Pt(CN)_4]Br_{0.3}\cdot 3H_2O$; TTF, tetrathiafulvalene; TCNQ, tetracyanoquinodimethane; TMTSF, tetramethyltetraselenafulvalene; BEDT-TTF, bis(ethylenedithio)tetrathiafulvalene; H_2dmit, 4,5-dimercapto-1,3-dithiol-2-thione; DBTTF, dibenzotetrathiafulvalene; DETCNQ, 2,5-diethyltetracyanoquinodimethane.

(6) Zeller, H. R. *Festkoerperprobleme* **1973**, *13*, 31-58.

(7) (a) Walatka, V. V.; Labes, M. M.; Perlstein, J. H. *Phys. Rev. Lett.* **1973**, *31*, 1139-1141. (b) Street, G. B.; Greene, R. L. *IBM J. Res. Dev.* **1977**, *21*, 99-110.

(8) (a) Alcacer, L.; Maki, A. *J. Phys. Chem.* **1974**, *78*, 215-217. (b) Ahmad, M. M.; Underhill, A. *J. Chem. Soc., Dalton Trans.* **1982**, 1065-1069.

(9) Heeger, A. J.; McDiarmid, A. G. in ref 3c, pp 353-391.

(10) Peierls, R. E. "Quantum Theory of Solids"; Clarendon Press: Oxford, 1955.

(11) (a) Bechgaard, K.; Carneiro, K.; Rasmussen, F. B.; Olsen, M.; Rindorf, G.; Jacobsen, C. S.; Pedersen, H. J.; Scott, J. C. *J. Am. Chem. Soc.* **1981**, *103*, 2440-2442. (b) Bechgaard, K.; Carneiro, K.; Olsen, M.; Rasmussen, F. B.; Jacobsen, C. S. *Phys. Rev. Lett.* **1981**, *46*, 852-855.

0002-7863/86/1508-1908$01.50/0

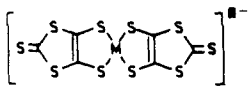

Figure 1. $[M(dmit)_2]^{n-}$ complexes.

Among the more effective strategies for enhancing interchain interaction has been the incorporation of additional sulfur or selenium atoms on the periphery of donor molecules such as TTF and tetraselenafulvalene (TSeF) in mixed-valence salts of these molecules.[13-20] An example is bis(ethylenedithio)tetrathiafulvalene (BEDT-TTF) where four additional sulfur atoms have been attached to TTF in the 4,5- and 4',5'-positions. The $(BEDT\text{-}TTF)_2I_3$ salt has been found to undergo a transition to a superconducting state at 1.4–1.6 K at ambient pressure,[12,14] and a mixed I/Br trihalide has recently been discovered which has a critical temperature for superconductivity of 2.7 K with evidence of a metastable phase which superconducts at 4.2 K.[15c]

Among the metal complex systems, the number of well-substantiated examples of molecular metals has been rather limited and to date none of these compounds has been found to undergo a transition to a superconducting state. We have recently reported the preparation and study of a series of metal complexes of the bis(dithiolene) ligand, 4,5-dimercapto-1,3-dithiol-2-thione (H_2dmit) in which high conductivity has been identified.[18] The molecular structure of these complexes (Figure 1) shares some common features with the BEDT-TTF system including the presence of peripheral sulfur atoms which are likely to appreciably extend the frontier orbitals of the bis(dithiolene) unit. The ability of these sulfur atoms to enhance interstack interactions has been evidenced in studies of both mixed-valence salts and donor–acceptor derivatives of this complex where the existence of *two-dimensional* electronic interactions is indicated by electrical conductivity measurements on single-crystal samples.[18-20]

We report here in detail the chemical and electrochemical synthesis, the crystal structure, and electrical properties of the donor–acceptor compounds formed by the $[M(dmit)_2]^{n-}$ complexes (M = Ni, Pd, and Pt) with the donor molecule TTF. A preliminary account of the work on the nickel derivative has been previously published.[21]

Experimental Section

Starting Materials. The $dmit^{2-}$ ligand has been prepared following the detailed procedure described in ref 18b. The $(n\text{-}Bu_4N)_n[M(dmit)_2]$ complexes (M = Ni, Pd, and Pt; n = 1 and 2) have been prepared following the procedures described by Steimecke.[22] The $(TTF)_3(BF_4)_2$ salt was prepared as described by Wudl.[23] All solvents were reagent-grade and freshly distilled and deaerated prior to use.

Synthesis of the $TTF[M(dmit)_2]_x$ Compounds (M = Ni, Pd, and Pt). Metathesis reaction under inert atmosphere of acetonitrile solutions of $(TTF)_3(BF_4)_2$ and the appropriate metal salt $(n\text{-}Bu_4N)[M(dmit)_2]$ (or $(n\text{-}Bu_4N)_2[M(dmit)_2]$) immediately yields insoluble, black, shiny microcrystalline powders. In two cases (M = Ni and Pd), a compound of stoichiometric $TTF[M(dmit)_2]_2$ was obtained. Anal. Calcd for $C_{18}H_4Ni_2S_{24}$: C, 19.53; H, 0.36; Ni, 10.61; S, 62.50. Found: C, 19.50; H, 0.40; Ni, 10.10; S, 62.90. Anal. Calcd for $C_{18}H_4Pd_2S_{24}$: C, 17.98; H, 0.33; Pd, 17.69; S, 63.99. Found: C, 18.35; H, 0.48; Pd, 17.42; S, 63.94. For M = Pt, a compound of stoichiometric $TTF[Pt(dmit)_2]_3$ was obtained. Anal. Calcd for $C_{24}H_4Pt_3S_{34}$: C, 14.64; H, 0.20; Pt, 29.74; S, 55.40. Found: C, 14.80; H, 0.3; Pt, 29.3; S, 55.70.

Crystal Growth of $TTF[M(dmit)_2]_x$ Compounds. All three compounds are virtually insoluble in common solvents, precluding their recyrstallization from solution. Single crystals suitable for conductivity measurements and X-ray diffraction studies were obtained by slow interdiffusion of saturated solutions of $(TTF)_3(BF_4)_2$ and $(n\text{-}Bu_4N)[M(dmit)_2]$. These experiments were carried out under an inert atmosphere in a three-compartment "H-tube" with a central solvent chamber and porous glass frits between compartments.[24] The concentration of the solution was kept close to saturation during the entire diffusion process. This was accomplished by means of additional containers filled with an excess of solid starting reagent, placed in the appropriate compartment and communicating with it through a high porosity glass frit. The design of this cell can be found in the supplementary material.[25] The cell was set in a thermostated dark chamber for 10–30 days at a temperature of 30–46 °C.

In the case of the nickel derivative, the best and largest crystals were obtained in acetonitrile at a temperature of 40 °C after a 15-day period. All experiments gave a mixture of fine needles (maximum size: 1 × 0.1 × 0.02 mm^3) and a few platelets. The latter were identified as crystals of the neutral $[Ni(dmit)_2]^0$ species by means of an X-ray diffraction study.[18b] The needlelike crystals were identified by elemental analysis, electron microprobe analysis, and comparison of X-ray powder diagrams as identical with the $TTF[Ni(dmit)_2]_2$ powder obtained as described above. Finally, this formula was confirmed by the crystal structure determination (vide infra).

In the case of the palladium derivative, only needlelike crystals were obtained (maximum size: 1 × 0.08 × 0.01 mm^3). The powder diagrams of these crystals and of the microcrystalline sample obtained by rapid mixing of the solutions of the component molecules are different (supplementary material[25]). Comparison of the diffraction data indicates that the needlelike phase is isomorphous with $TTF[Ni(dmit)_2]_2$.

The platinum derivative also gave needlelike crystals (maximum size: 1.1 × 0.04 × 0.007 mm^3). Powder diagrams of this phase and of the microcrystalline sample obtained by rapid mixing of the component solutions are identical (supplementary material[25]). Finally, the formula of the needlelike species obtained by the diffusion technique was unambiguously established as $TTF[Pt(dmit)_2]_3$ by the crystal structure determination (vide infra).

Electrochemical Synthesis of $TTF[Ni(dmit)_2]_2$. Crystals of $TTF[Ni(dmit)_2]_2$ may also be obtained by galvanostatic electrolysis of an acetonitrile solution containing $(n\text{-}Bu_4N)[Ni(dmit)_2]$ and a large excess of neutral TTF.[26] A nitrogen-flushed U-type cell where the anode and cathode are separated by a medium-porosity glass frit was used with platinum electrodes. The cell was thermostated (20 °C) and the current (I = 5 μA; current density = 5 × 10^{-5} A cm^{-2}) was held constant. Black needlelike crystals formed on the anode were collected on a glass frit by filtration, washed with acetonitrile, and vacuum-dried. The powder diagram of these crystals was identical with that of the needlelike $[TTF\,Ni(dmit)_2]_2$ crystals isolated from the diffusion experiment. However, the electrochemically synthetized crystals were inferior in size and quality.

Physical Measurements. Four probe conductivity measurements were carried out by using a Keithley 225 dc current source and a Keithley 616

(12) Yagubskii, E. B.; Shchegolev, I. F.; Laukhin, V. N.; Kononovich, P. A.; Karatsovnik, M. V.; Zvarykina, A. V.; Buravov, L. I. *Pis'ma Zh. Eksp. Teor. Fiz.* **1984**, *39*, 12–15 (*JETP Lett. (Engl. Transl.)* **1984**, *39*, 12–16).
(13) Saito, G.; Enoki, T.; Toriumi, K.; Inokuchi, H. *Solid State Commun.* **1982**, *42*, 557–560.
(14) (a) Wudl, F. *J. Am. Chem. Soc.* **1981**, *103*, 7064–7069. (b) Rindorf, G.; Soling, H.; Thorup, N. *Acta Crystallogr., Sect. B* **1982**, *B38*, 2805–2808. (c) Beno, M. A.; Williams, J. M.; Lee, M. M.; Cowan, D. O. *Solid State Commun.* **1982**, *44*, 1195–1199.
(15) (a) Kaminski, V. F.; Prokhorova, T. G.; Shibaeva, R. P.; Yagubskii, E. B. *Pis'ma Zh. Eksp. Teor. Fiz.* **1984**, *39*, 15–18 (*JETP Lett. (Engl. Transl.)* **1984**, *39*, 17–20). (b) Kobayashi, H.; Kobayashi, A.; Sasaki, Y.; Saito, G.; Enoki, T.; Inokuchi, H. *J. Am. Chem. Soc.* **1983**, *105*, 297–298. (c) Williams, J. M.; Wang, H. H.; Beno, M. A.; Emge, T. J.; Sowa, L. M.; Copps, P. T.; Behroozi, F.; Hall, L. N.; Carlson, K. D.; Crabtree, G. W. *Inorg. Chem.* **1984**, *23*, 3839–3841.
(16) Wudl, F. *Pure Appl. Chem.* **1982**, *54*, 1051–1058.
(17) Valade, L.; Bousseau, M.; Cassoux, P. *Nouv. J. Chim.* **1985**, *9*, 351–357.
(18) (a) Valade, L.; Bousseau, M.; Gleizes, A.; Cassoux, P. *J. Chem. Soc., Chem. Commun.* **1983**, 110–112. (b) Valade, L.; Legros, J.-P.; Bousseau, M.; Cassoux, P.; Garbauskas, M.; Interrante, L. V. *J. Chem. Soc., Dalton Trans.* **1985**, 783–794. (c) Cassoux, P.; Valade, L.; Bousseau, M.; Legros, J. P.; Garbauskas, M.; Interrante, L. *J. Mol. Cryst. Liq. Cryst.* **1985**, *20*, 377–380.
(19) Kato, R.; Mori, T.; Kobayashi, A.; Sasaki, Y.; Kobayashi, H. *Chem. Lett.* **1984**, 1–4.
(20) (a) Kato, R.; Kobayashi, H.; Kobayashi, A.; Sasaki, Y. *Chem. Lett.* **1985**, 131–134. (b) Kobayashi, H.; Kato, R.; Kobayashi, A.; Sasaki, Y. *Ibid.* **1985**, 191–194. (c) Kobayashi, H.; Kato, R.; Kobayashi, A.; Sasaki, Y. *Ibid* **1985**, 535–538.
(21) Bousseau, M.; Valade, L.; Bruniquel, M.-F.; Cassoux, P.; Garbauskas, M.; Interrante, L.; Kasper, J. *Nouv. J. Chim.* **1984**, *8*, 3–6.
(22) (a) Steimecke, G. PhD Thesis, Leipzig, GDR, 1977. (b) Steimecke, G.; Sieler, H. J.; Kirmse, R.; Hoyer, E. *Phosphorus Sulfur* **1979**, *7*, 49–55.
(23) Wudl, F. *J. Am. Chem. Soc.* **1975**, *97*, 1962-1964.
(24) (a) Andersen, J. R.; Engler, E. M.; Bechgaard, K. *Ann. N. Y. Acad. Sci. U.S.A.* **1978**, *313*, 293–300. (b) Anzai, J. *J. Cryst. Growth* **1976**, *33*, 185–188. (c) Kaplan, M. L. *Ibid.* **1976**, *33*, 161–164.
(25) Supplementary material.
(26) On the basis of the respective oxidation potentials (0.21 V vs. SCE for $[Ni(dmit)_2]^-$ and 0.33 V vs. SCE for TTF), the oxidation of a stoichiometric mixture of $(n\text{-}Bu_4N)[Ni(dmit)_2]$ and neutral TTF would not be expected to give a charge-transfer compound. Instead, one should obtain the mixed-valence salt $(n\text{-}Bu_4N)_{0.29}[Ni(dmit)_2]$, as described in ref 18b. This difficulty was apparently overcome by using a very large excess of TTF and setting the electrolysis current to a higher value than the oxidation peak current of $(n\text{-}Bu_4N)[Ni(dmit)_2]$.

Table I. Crystal Data, Data Collection, and Reduction Parameters

compound	$TTF[Ni(dmit)_2]_2$	$TTF[Pt(dmit)_2]_3$
formula, M_w	$C_{18}H_4Ni_2S_{24}$, 1107.19	$C_{24}H_4Pt_3S_{34}$, 1967.74
crystal system, space group	monoclinic, $C2/c$	triclinic, $P\bar{1}$
crystal dimensions, mm^3	0.5 × 0.1 × 0.02	0.4 × 0.1 × 0.01
a, Å	46.22 (3)	6.314 (5)
b, Å	3.732 (2)	11.66 (2)
c, Å	22.86 (1)	16.81 (3)
α, deg	90	84.5 (1)
β, deg	119.3 (1)	89.6 (1)
γ, deg	90	81.9 (1)
V, Å^3	3439	1220
Z	4	1
d_{calcd}, g cm^{-3}	2.14	2.68
$F(000)$	552	926
radiation λ (Å), temp (K)	Mo Kᾱ 0.710 69,293	same
μ(Mo Kᾱ), cm^{-1}	25.24	70.31
scan mode	$\omega/2\theta$, variable scan speed	same
2θ range, deg	$3 \leq 2\theta \leq 45$	$4 \leq 2\theta \leq 45$
hkl range	$0 \leq h \leq 50$, $0 \leq k \leq 5$, $-25 \leq l \leq 25$ with h + k = 2n	$0 \leq h \leq 7$, $-12 \leq k \leq 12$, $-17 \leq l \leq 17$
no. of intensity meas.	2687	2744
criterion for obsd reflections	$F > 2.5\sigma(F)$	$F > 3\sigma(F)$
no. of independent obsd reflections	1475	1535
no. of refined parameters	154	220
weighting scheme w^{-1}	$\sigma^2(F) + 0.005F^2$	$\sigma^2(F) + 0.002F^2$
$R = \sum(\|\|F_o\| - \|F_c\|\|)/\sum\|F_o\|$	0.097	0.101
$R_w = [\sum w(\|F_o\| - \|F_c\|)^2/\sum wF_o^2]^{1/2}$	0.117	0.110

electrometer or a Hewlett-Packard 3490 A multimeter. Ac measurements were also carried out by using a RV Elektroniika Oy, AVS45-L automatic resistance bridge. Both dc and ac measurements gave the same results. The mounting of the crystals and the temperature control devices have been described previously.[18b] Measurements for each species were performed on between 5 and 10 different crystals from different batches and gave consistent results.

Elemental analysis were performed at the L.C.C. (C, H, and N) and at the Service Central de Microanalyses du CNRS (Ni, Pd, Pt, and S). Electron microprobe analyses were performed on a CAMECA MS46 camera. A Siemens goniometer utilizing monochromatized copper radiation was used for X-ray powder patterns.

Crystal Structure Determinations. All single-crystal measurements were made with a Nicolet P3F automatic diffractometer. Numerical details for the two crystallographic analyses are presented in Table I. Accurate unit cell parameters were derived from a least-squares refinement based on the setting angles of 25 reflections. The structures were solved by direct methods and/or Patterson techniques and refined by using a block-diagonal least-squares procedure. The function minimized was $\sum w(|F_o| - |F_c|)^2$ where $|F_o|$ and $|F_c|$ and $|F_c|$ are the scaled observed and calculated structure factor amplitudes. The programs used are part of the standard software (SHELXTL program package) of the diffractometer and run on a Data General Eclipse S/140 computer. The atomic scattering factors and anomalous dispersion corrections were taken from "International Tables for X-ray Crystallography".[27a] No absorption correction was applied.[27b] Details specific to each of the structure determinations are presented below.

Crystal Structure of $TTF[Ni(dmit)_2]_2$. The Ni and S atoms were refined anisotropically. All C atoms were refined isotropically. All H atoms were included in calculated positions (C–H = 1.0 Å). Atomic coordinates are listed in Table II; the atoms are labeled according to Figure 2. Bond lengths are listed in Table III and bond angles in Table IV. Observed and calculated structure factor amplitudes, thermal parameters, and hydrogen coordinates are available as supplementary material.[25]

Table II. $TTF[Ni(dmit)_2]_2$—Fractional Atomic Coordinates of Non-Hydrogen Atoms with Estimated Standard Deviations in Parentheses

atom	x/a	y/b	z/c
Ni	0.2887 (1)	0.6560 (8)	0.4306 (1)
S(1)	0.2434 (1)	0.487 (2)	0.4292 (2)
S(2)	0.1721 (1)	0.482 (2)	0.3182 (2)
S(3)	0.1195 (1)	0.622 (2)	0.1773 (3)
S(4)	0.1897 (1)	0.787 (1)	0.2228 (2)
S(5)	0.2624 (1)	0.792 (1)	0.3252 (2)
S(6)	0.3150 (1)	0.540 (2)	0.5373 (2)
S(7)	0.3878 (1)	0.609 (2)	0.6402 (2)
S(8)	0.4574 (1)	0.807 (2)	0.6833 (2)
S(9)	0.4045 (1)	0.879 (2)	0.5416 (2)
S(10)	0.3334 (1)	0.817 (2)	0.4294 (2)
S(11)	0.0495 (1)	0.099 (2)	0.0831 (3)
S(12)	−0.0155 (1)	0.089 (2)	0.0750 (3)
C(1)	0.2143 (4)	0.566 (5)	0.3493 (7)
C(2)	0.1590 (4)	0.624 (6)	0.2372 (9)
C(3)	0.2217 (4)	0.709 (5)	0.3023 (8)
C(4)	0.3548 (4)	0.638 (5)	0.5593 (8)
C(5)	0.4196 (5)	0.768 (5)	0.6276 (9)
C(6)	0.3646 (4)	0.765 (5)	0.5124 (8)
C(7)	0.0073 (5)	0.036 (6)	0.0327 (9)
C(8)	0.0477 (6)	0.169 (7)	0.157 (1)
C(9)	0.0188 (5)	0.176 (7)	0.157 (1)

Table III. $TTF[Ni(dmit)_2]_2$—Bond Lengths (Å) with Estimated Standard Deviations in Parentheses. a Refers to the Transformation $-x,-y,-z$

Ni–S(1)	2.172 (8)	Ni–S(5)	2.161 (6)
Ni–S(6)	2.170 (6)	Ni–S(10)	2.164 (8)
S(1)–C(1)	1.68 (1)	S(2)–C(1)	1.75 (2)
S(2)–C(2)	1.73 (2)	S(3)–C(2)	1.66 (2)
S(4)–C(2)	1.72 (2)	S(4)–C(3)	1.72 (1)
S(5)–C(3)	1.72 (2)	S(6)–C(4)	1.69 (2)
S(7)–C(4)	1.73 (2)	S(7)–C(5)	1.73 (3)
S(8)–C(5)	1.59 (2)	S(9)–C(5)	1.78 (2)
S(9)–C(6)	1.68 (6)	S(10)–C(6)	1.74 (2)
S(11)–C(7)	1.73 (2)	S(11)–C(8)	1.76 (3)
S(12)–C(7)	1.76 (3)	S(12)–C(9)	1.73 (2)
C(1)–C(3)	1.39 (3)	C(4)–C(6)	1.44 (3)
C(7)–C(7a)	1.33 (4)	C(8)–C(9)	1.28 (4)

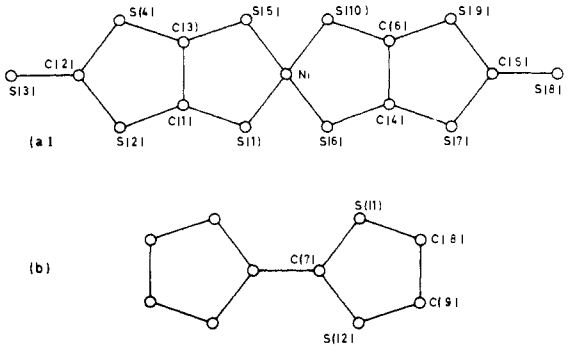

Figure 2. Atom labeling scheme for $TTF[Ni(dmit)_2]_2$.

Crystal Structure of $TTF[Pt(dmit)_2]_3$. The structure determination was initially carried out in the $P1$ space group and then in the $P\bar{1}$ space group when symmetry was observed. The $P\bar{1}$ space group was confirmed by the usual statistical tests. Pt and S atoms were refined anisotropically. All C atoms were refined isotropically. H atoms were not included in structure factor calculations. Atomic coordinates are listed in Table V; the atoms are labeled according to Figure 3. Bond lengths are listed in Table VI and bond angles in Table VII. Observed and calculated structure factor amplitudes and thermal parameters are available as supplementary material.[25]

Phase Transitions of $TTF[Pd(dmit)_2]_2$. The intensities of five of the most intense reflections were measured repeatedly, using a CAD4 Enraf

(27) (a) "International Tables for X-ray Crystallography"; Kynoch Press: Birmingham, England, 1974; Vol. IV. (b) As can be seen from Table I, the crystals employed in both cases were thin needles, suggesting that an absorption correction should be applied; however, it was estimated that no significant improvement would have been gained on applying these corrections for the following reasons: in the case of the $TTF[Pt(dmit)_2]_3$ system, the available crystals were so small and weakly diffracting that there was insufficient data to carry out a refinement with all atoms anisotropic. It was felt that with the intensities so low, the standard deviations in these intensities were large enough to make an absorption correction questionable. The $TTF[Ni(dmit)_2]_2$ crystals also gave relatively low intensities; however, in this case, measurement of the merging R for the data obtained gave a value of about 3%. This, coupled with the moderate absorption coefficient of 25 cm^{-1}, indicated that the absorption correction would be small and, therefore, unnecessary.

Table IV. $TTF[Ni(dmit)_2]_2$—Bond Angles (deg) with the Estimated Standard Deviations in Parentheses. a Refers to the Transformation $-x,-y,-z$

S(1)-Ni-S(5)	92.2 (5)	S(1)Ni-S(6)	88 (2)
S(5)-Ni-S(6)	177.9 (3)	S(1)-Ni-S(10)	178.5 (3)
S(5)-Ni-S(10)	86.6 (2)	S(6)-Ni-S(10)	93.3 (2)
Ni-S(1)-C(1)	102.7 (7)	C(1)-S(2)-C(2)	96.7 (9)
C(2)-S(4)-C(3)	95.9 (9)	Ni-S(5)-C(3)	103.5 (7)
Ni-S(6)-C(4)	102.8 (7)	C(4)-S(7)-C(5)	100 (1)
C(5)-S(9)-C(6)	98 (1)	Ni-S(10)-C(6)	104.0 (8)
C(7)-S(11)-C(8)	95 (1)	C(7)-S(12)-C(9)	95 (1)
S(1)-C(1)-S(2)	123 (1)	S(1)-C(1)-C(3)	123 (1)
S(2)-C(1)-C(3)	114 (1)	S(2)-C(2)-S(3)	123 (2)
S(2)-C(2)-S(4)	115.2 (9)	S(3)-C(2)-S(4)	121 (1)
S(4)-C(3)-S(5)	123 (1)	S(4)-C(3)-C(1)	118 (3)
S(5)-C(3)-C(1)	119 (1)	S(6)-C(4)-S(7)	125 (1)
S(6)-C(4)-C(6)	123 (1)	S(7)-C(4)-C(6)	113 (1)
S(7)-C(5)-S(8)	126 (1)	S(7)-C(5)-S(9)	110.9 (9)
S(8)-C(5)-S(9)	123 (2)	S(9)-C(6)-S(10)	125 (1)
S(9)-C(6)-C(4)	118 (1)	S(10)-C(6)-C(4)	117 (1)
S(11)-C(7)-S(12)	114 (1)	S(11)-C(7)-C(7a)	124 (3)
S(12)-C(7)-C(7a)	122 (2)	S(11)-C(8)-C(9)	117 (2)
S(12)-C(9)-C(8)	120.0 (2)		

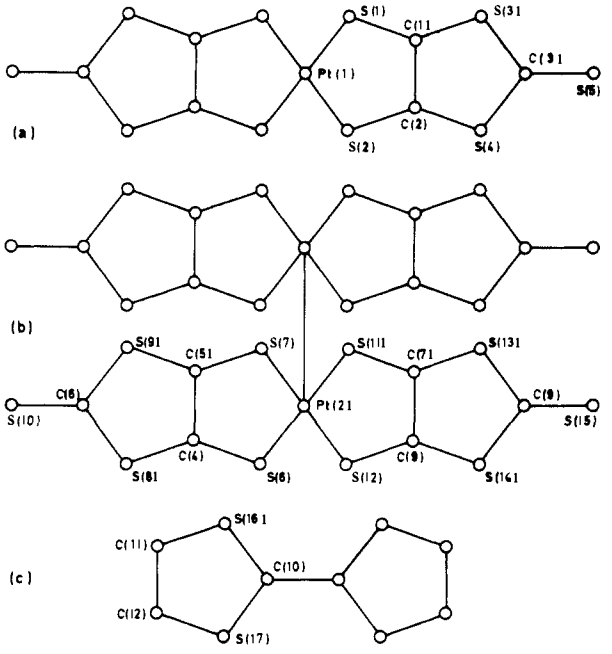

Figure 3. Atom labeling scheme for $TTF[Pt(dmit)_2]_3$: (a) the $Pt(dmit)_2$ monomer, (b) the $[Pt(dmit)_2]_2$ dimer, and (c) the TTF molecule.

Nonius diffractometer equipped with a nitrogen gas flow cooling device. While a crystal was cooled down to 120 K and then warmed up back to room temperature, phase transitions were observed from abrupt changes in the intensities. The unit cell parameters of the various phases were determined at 293 and 120 K from a least-squares refinement based on the setting angles of 25 reflections.

Results

Stoichiometry of the $TTF[M(dmit)_2]_x$ Phases. On rapid mixing of solutions of $(TTF)_3(BF_4)_2$ and the appropriate $(n\text{-}Bu_4N)[M(dmit)_2]$ salt, species of different stoichiometry were obtained depending on the nature of the metal: $x = 2$ for M = Ni and Pd and $x = 3$ for M = Pt. All these species exhibit a high compaction powder conductivity: ca. 50, ca. 30, and ca. 1 Ω^{-1} cm^{-1}, for M = Ni, Pd, and Pt, respectively.

Single crystals of these three compounds were obtained by a solution diffusion technique. However, such a technique may yield different species or a heterogeneous sample, and special attention must be devoted to careful characterization of the crystals used for further determination. In the case of the platinum derivative, comparison of X-ray powder patterns[25] has shown that the same $TTF[Pt(dmit)_2]_3$ phase has been obtained by both rapid mixing and diffusion techniques. In the case of the nickel derivative, the diffusion technique yielded, in addition to a majority of needlelike $TTF[Ni(dmit)_2]_2$ crystals, a few crystals (platelets) that could be sorted out and identified as the nonconductive neutral $[Ni(dmit)_2]^0$ species;[18b] this indicates that in such a slow process, the total oxidation of a small amount of the $(n\text{-}Bu_4N)[M(dmit)_2]$ salt is possible. However, the occurrence of the $[Ni(dmit)_2]^0$ neutral phase seems to be aleatory, and no clear relationship with the experimental conditions (temperature, time, and nature of solvent) was noted.

The crystals of $TTF[Ni(dmit)_2]_2$ obtained by the electrochemical method from an excess of neutral TTF and $(n\text{-}Bu_4N)[Ni(dmit)_2]$ are identical to the needlelike crystals obtained by the diffusion technique. However, the electrochemical method is more selective and yields homogeneous samples.

In the case of the palladium derivative, two crystallographically different phases with the same $TTF[Pd(dmit)_2]_2$ stoichiometry were obtained, depending on whether rapid mixing or the diffusion

Table V. $TTF[Pt(dmit)_2]_3$—Fractional Atomic Coordinates of Non-Hydrogen Atoms with Estimated Standard Deviations in Parentheses

atom	x/a	y/b	z/c
Pt(1)	0	0	0
Pt(2)	-0.4119 (2)	0.3893 (2)	0.0445 (1)
S(1)	-0.308 (2)	0.008 (1)	0.0737 (8)
S(2)	0.143 (2)	0.109 (1)	0.0876 (7)
S(3)	-0.422 (2)	0.109 (1)	0.2296 (8)
S(4)	-0.015 (2)	0.196 (1)	0.2408 (8)
S(5)	-0.338 (2)	0.240 (1)	0.3682 (9)
S(6)	-0.712 (2)	0.379 (1)	0.1234 (7)
S(7)	-0.263 (2)	0.482 (1)	0.1417 (8)
S(8)	-0.825 (2)	0.457 (1)	0.2849 (8)
S(9)	-0.426 (2)	0.554 (1)	0.2990 (8)
S(10)	-0.745 (2)	0.571 (1)	0.431 (1)
S(11)	-0.096 (2)	0.377 (1)	-0.258 (7)
S(12)	-0.544 (2)	0.275 (1)	-0.0429 (7)
S(13)	0.044 (2)	0.266 (1)	-0.1749 (7)
S(14)	-0.360 (2)	0.171 (1)	-0.1896 (8)
S(15)	-0.017 (2)	0.129 (1)	-0.3106 (9)
S(16)	0.504 (2)	0.159 (1)	0.560 (1)
S(17)	0.206 (2)	0.092 (1)	0.446 (1)
C(1)	-0.247 (6)	0.077 (3)	0.157 (2)
C(2)	-0.047 (7)	0.127 (4)	0.152 (3)
C(3)	-0.264 (6)	0.183 (4)	0.284 (3)
C(4)	-0.654 (8)	0.443 (4)	0.209 (3)
C(5)	-0.463 (8)	0.491 (5)	0.213 (3)
C(6)	-0.678 (7)	0.528 (4)	0.343 (3)
C(7)	-0.137 (6)	0.290 (3)	-0.101 (2)
C(8)	-0.342 (5)	0.251 (3)	-0.105 (2)
C(9)	-0.114 (7)	0.188 (4)	-0.231 (3)
C(10)	0.441 (7)	0.054 (4)	0.504 (3)
C(11)	0.286 (9)	0.264 (5)	0.524 (4)
C(12)	0.147 (7)	0.233 (4)	0.479 (3)

Table VI. $TTF[Pt(dmit)_2]_3$—Bond Lengths (Å) with Estimated Standard Deviations in Parentheses. Lower-Case Letters Refer to the Transformations (a) $-1-x,1-y,-z$ and (b) $1-x,-y,1-z$

Pt(1)-S(1)	2.29 (1)	Pt(1)-S(2)	2.30 (1)
Pt(2)-S(6)	2.32 (1)	Pt(2)-S(7)	2.32 (1)
Pt(2)-S(11)	2.30 (1)	Pt(2)-S(12)	2.31 (1)
S(1)-C(1)	1.74 (4)	S(2)-C(2)	1.62 (5)
S(3)-C(1)	1.68 (4)	S(3)-C(3)	1.72 (5)
S(4)-C(2)	1.79 (5)	S(4)-C(3)	1.75 (4)
S(5)-C(3)	1.67 (5)	S(6)-C(4)	1.75 (6)
S(7)-C(5)	1.73 (6)	S(8)-C(4)	1.67 (5)
S(8)-C(6)	1.70 (5)	S(9)-C(5)	1.72 (6)
S(9)-C(6)	1.80 (5)	S(10)-C(6)	1.63 (5)
S(11)-C(7)	1.73 (4)	S(12)-C(8)	1.65 (3)
S(13)C(7)	1.70 (8)	S(13)-C(9)	1.77 (5)
S(14)-C(8)	1.79 (4)	S(14)-C(9)	1.73 (5)
S(15)-C(9)	1.64 (5)	S(16)-C(10)	1.70 (6)
S(16)-C(11)	1.78 (5)	S(17)-C(10)	1.76 (5)
S(17)-C(12)	1.77 (5)	C(1)-C(2)	1.46 (6)
C(4)-C(5)	1.41 (8)	C(7)-C(8)	1.44 (5)
C(10)-C(10b)	1.40 (9)	C(11)-C(12)	1.28 (8)
Pt(2)-Pt(2a)	2.935 (3)		

Table VII. $TTF(Pt(dmit)_2]_3$—Bond Angles (deg) with the Estimated Standard Deviations in Parentheses. Lower-Case Letters Refer to the Transformations (a) $-1-x,1-y,-z$ and (b) $1-x,-y,1-z$

S(1)-Pt(1)-S(2)	90.1 (4)		
Pt(2a)-Pt(2)-S(6)	94.2 (3)	Pt(2a)-Pt(2)-S(7)	92.5 (3)
S(6)-Pt(2)-S(7)	89.3 (4)	Pt(2a)-Pt(2)-S(11)	93.1 (3)
S(6)-Pt(2)-S(11)	172.7 (4)	S(7)-Pt(2)-S(11)	90.7 (4)
Pt(2a)-Pt(2)-S(12)	94.8 (3)	S(6)-Pt(2)-S(12)	89.8 (4)
S(7)-Pt(2)-S(12)	172.7 (4)	S(11)-Pt(2)-S(12)	89.2 (4)
Pt(1)-S(1)-C(1)	104 (1)	Pt(1)-S(2)-C(2)	101 (2)
C(1)-S(3)-C(3)	98 (2)	C(2)-S(4)-C(3)	99 (2)
S(1)-C(1)-S(3)	124 (2)	S(1)-C(1)C(2)	116 (3)
S(3)-C(1)-C(2)	119 (3)	S(2)-C(2)-S(4)	121 (3)
S(2)-C(2)-C(1)	128 (4)	S(4)-C(2)-C(1)	110 (3)
S(4)-C(3)-S(5)	122 (3)	S(4)-C(3)-S(3)	114 (3)
S(5)-C(3)-S(3)	125 (3)	C(4)-S(6)-Pt(2)	104 (2)
C(5)-S(7)-Pt(2)	102 (2)	C(4)-S(8)-C(6)	98 (3)
C(5)-S(9)-C(6)	96 (6)	S(6)C(4)-S(8)	123 (3)
S(6)-C(4)-C(5)	119 (4)	S(8)-C(4)-C(5)	118 (4)
S(7)-C(5)-S(9)	120 (3)	S(7)-C(5)-C(4)	125 (4)
S(9)-C(5)-C(4)	115 (4)	S(8)-C(6)-S(9)	113 (3)
S(8)-C(6)-S(10)	127 (3)	S(9)-C(6)-S(10)	120 (3)
C(7)-S(11)-Pt(2)	104 (1)	C(8)-S(12)-Pt(2)	102 (1)
C(7)-S(13)-C(9)	96 (2)	C(8)-S(14)-C(9)	98 (2)
S(11)-C(7)-S(13)	122 (2)	S(11)-C(7)-C(8)	118 (3)
S(13)-C(7)-C(8)	120 (3)	S(12)-C(8)-S(14)	122 (2)
S(12)-C(8)-C(7)	127 (3)	S(14)-C(8)-C(7)	112 (2)
S(13)-C(9)-S(14)	115 (3)	S(13)-C(9)-S(15)	121 (3)
S(14)-C(9)-S(15)	125 (3)	C(10)-S(16)-C(11)	95 (3)
C(10)-S(17)-C(12)	95 (2)	S(16)-C(10)-S(17)	116 (3)
S(16)-C(10)-C(10b)	127 (5)	S(17)-C(10)-C(10b)	117 (5)
S(16)-C(11)-C(12)	119 (5)	S(17)-C(12)-C(11)	116 (4)

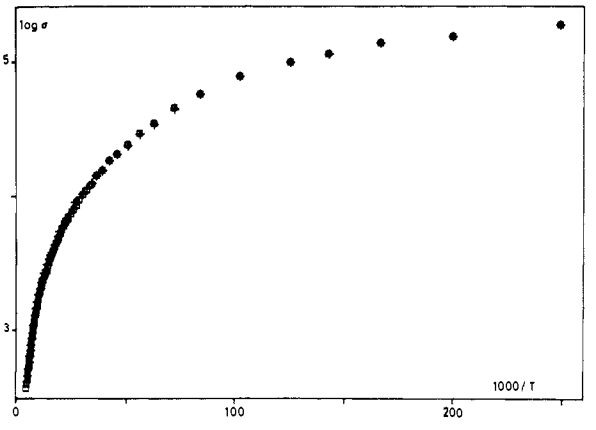

Figure 4. log conductivity vs. inverse of temperature for a crystal of $TTF[Ni(dmit)_2]_2$ between 300 and 4 K, measured on cooling (+) and subsequent warming (□).

technique was used. X-ray powder patterns[25] indicate that the needlelike crystals (diffusion) are isomorphous with $TTF[Ni(dmit)_2]_2$, thus confirming the stoichiometry of the crystals used for conductivity measurements.

$TTF[Ni(dmit)_2]_2$. The room-temperature electrical conductivity of $TTF[Ni(dmit)_2]_2$, measured along the needle axis, is very high: 300 Ω^{-1} cm^{-1} (the needle axis is parallel to the [010] direction).

$TTF[Ni(dmit)_2]_2$ exhibits a metallike conductivity behavior[28] throughout the entire range of temperatures investigated (300–4 K) (Figure 4). Unlike all previous examples of molecular metals,[2-4,11,12,16] the increase in conductivity with decreasing temperature does not peak or even saturate above 4 K. The conductivity at this temperature is ca. 1.5 10^5 Ω^{-1} cm^{-1} and the ratio $\sigma_{4K}/\sigma_{300K}$ is 500. Over the whole 300–4 K temperature range, the observed data can be fitted by $\sigma \propto T^{-1.6}$. As shown in Figure 4, this behavior is completely reversible on warming the sample back to 300 K. The magnitude of the conductivity observed at 4 K is among the highest observed for a molecular solid, and the sharply increasing conductivity at the lowest temperatures investigated could be suggestive of a metal in the paraconductive regime, just before a transition to a superconductive state.[29] At ambient pressures this prospect is apparently not realized, as is evidenced by magnetoresistance measurements[30a] which indicate a saturation of the conductivity near 2 K. Also, ratio frequency penetration depth measurements were carried out at temperatures as low as 0.49 K, and no superconducting transition was detected.[30b] However, recent resistivity studies have revealed a superconductive state at higher pressures for this compound, with a transition temperature of 1.62 K at 7 kbar.[30c]

The structure of $TTF[Ni(dmit)_2]_2$ can be described as segregated stacks along [010] of the donor (TTF) and acceptor $Ni(dmit)_2$ molecules (Figures 5 and 6; a stereoview of the unit cell content is available as supplementary material[25]). Both donor and acceptor entities are essentially planar.[25] However, the $Ni(dmit)_2$ units are slightly folded as indicated by the dihedral angle of 4.4° between the two Ni(dmit) moieties.[25] The spacing between stack sites is b = 3.73 Å, but both TTF and $Ni(dmit)_2$ units are tilted out of the (010) plane, resulting in somewhat shorter interplanar separations: due to the greater tilts of the $Ni(dmit)_2$ entities (18° relative to [010]), the mean interplanar spacing within the acceptor stacks is 3.55 Å, whereas the smaller tilt of the TTF molecular planes (12°) results in a significantly longer separation of 3.65 Å. This rather large interplanar separation results in intermolecular *intrastack* S···S distances larger than the sum of the corresponding van der Waals radii.[31]

On the other hand, a number of intermolecular *interstack* S···S contacts involving both types of molecules are appreciably shorter than the van der Waals separation of 3.70 Å.[31] Such S···S interactions as short as 3.45 Å are observed between $Ni(dmit)_2$ units in adjacent stacks (arranged along [001]) involving molecules at different levels along [010], such that a two-dimensional array of closely spaced molecules is formed in the (100) plane (Figure 6). Other even shorter S···S interactions (3.38 Å) are found between the terminal sulfur atoms of the $Ni(dmit)_2$ units and sulfur atoms in the TTF molecules, extending the range of interactions in the third direction (Figure 5). Thus, on the basis of these structural observations, $TTF[Ni(dmit)_2]_2$ appears to have a quasi-*three-dimensional* network of intermolecular S···S interactions.

$TTF[Pd(dmit)_2]_2$. The room-temperature conductivity of the palladium derivative, measured along the needle axis ([010]) is 750 Ω^{-1} cm^{-1}, even higher than the value observed for the nickel derivative.

$TTF[Pd(dmit)_2]_2$ exhibits a very "flat" metallike conductivity behavior when cooling the crystal to ca. 220 K ($\sigma_{220K}/\sigma_{300K}$ = 1.05). As shown in Figure 7, the conductivity saturates around 220 K and decreases below this temperature. This gradual metal-to-semiconductor transition has been observed at the same temperature of ca. 220 K for five different crystals from different batches. Below this temperature, in the semiconducting regime, the activation energy remains very low (0.01 eV). This transition seems to be irreversible, and on the subsequent first warming, second cooling, and second warming cycles, the crystal behaves as a semiconductor throughout the entire range of temperatures investigated (300–77 K). However, the room-temperature conductivity remains unchanged after several temperature cycles. Moreover, as shown in Figure 8, the metallike behavior of this

(28) In the preliminary communication on this work,[21] we had noted abrupt changes in resistance as some of the crystals were cooled to 4 K. These effects were attributed to small breaks in the crystal due to stresses induced in cooling the sample. This is now confirmed by additional results obtained for five crystals from two different batches which all give continuous conductivity vs. temperature curves. The most critical factor for obtaining such continuous curves is a very slow (1°/min or less) and regular temperature decrease (or increase) over the *entire* temperature range.

(29) (a) Soda, T. *Prog. Theor. Phys.* **1983**, *69*, 1060, (b) Aslamazov, L. G.; Larkin, A. I. *Sov. Phys.—Solid State (Engl. Transl.)* **1968**, *10*, 875.

(30) (a) Ulmet, J. P.; Auban, P.; Khmou, A.; Valade, L.; Cassoux, P. *Phys Lett.* **1985**, *113A*, 217–219. (b) Williams, J. M. Personal communication. (c) **Note Added in Proof**: Brossard, L.; Ribault, M.; Bousseau, M.; Valade, L.; Cassoux, P. *C. R. Acad. Sci. Paris. Ser. 2*, **1986**, *302*, 205–210.

(31) Pauling, L. "The Nature of the Chemical Bond"; Cornell University Press: Ithaca, NY, 1960.

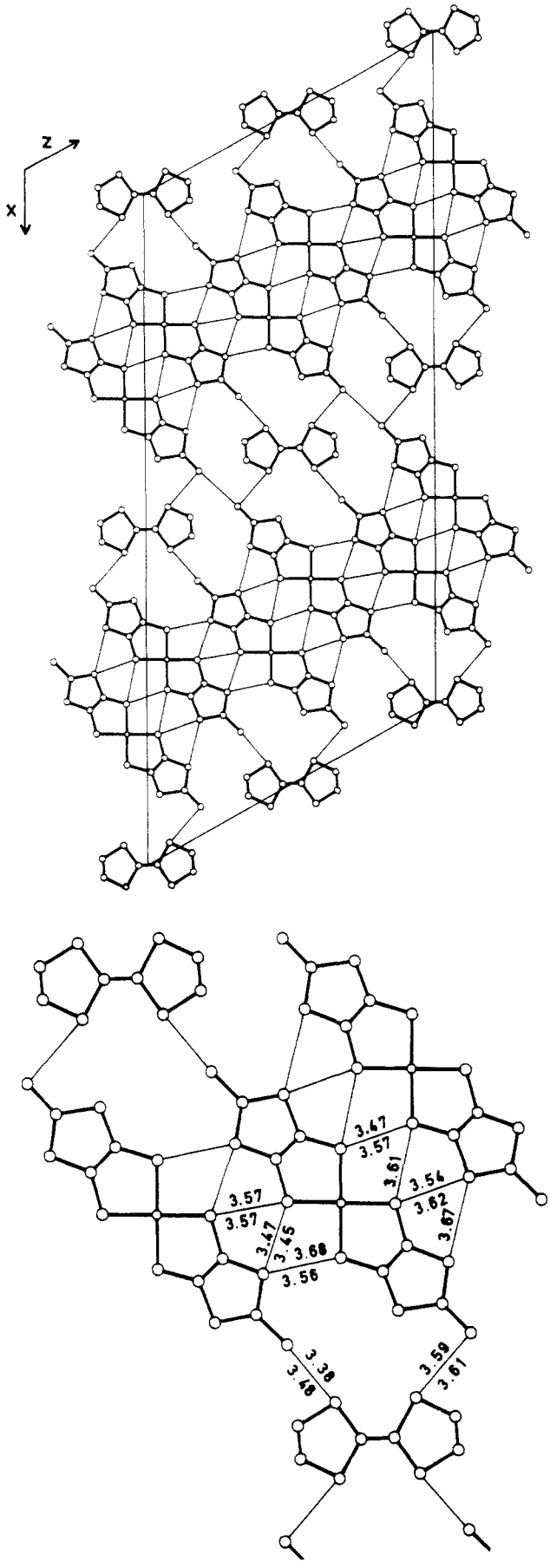

Figure 5. $TTF[Ni(dmit)_2]_2$. (a, top) Projection of the crystal structure onto the (010) plane. Thin lines indicate S···S distances shorter than 3.70 Å. (b, bottom) Blow up of a portion of this projection; crystallographically independent S···S distances (Å) are indicated.

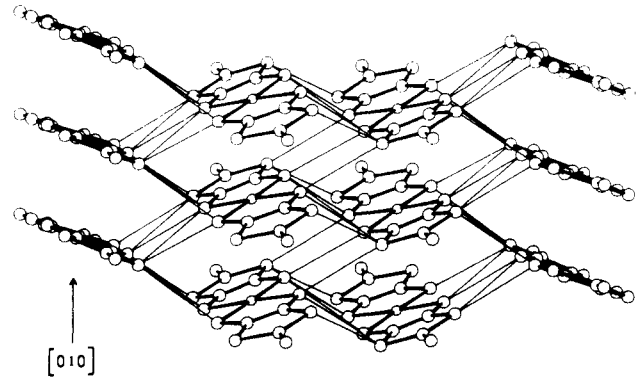

Figure 6. $TTF[Ni(dmit)_2]_2$. Parallel view of $Ni(dmit)_2$ entities stacked along [010]. Within a stack, the intermolecular separation is b. Thin lines indicate S···S distances shorter than 3.70 Å.

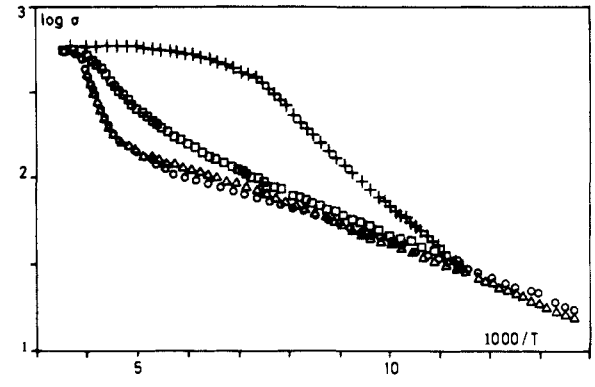

Figure 7. log conductivity vs. inverse of temperature for a crystal of $TTF[Pd(dmit)_2]_2$ between 300 and 77 K, on subsequent cooling and warming cycles: (+) first cooling, (□) first warming, (△) second cooling, and (○) second warming cycles.

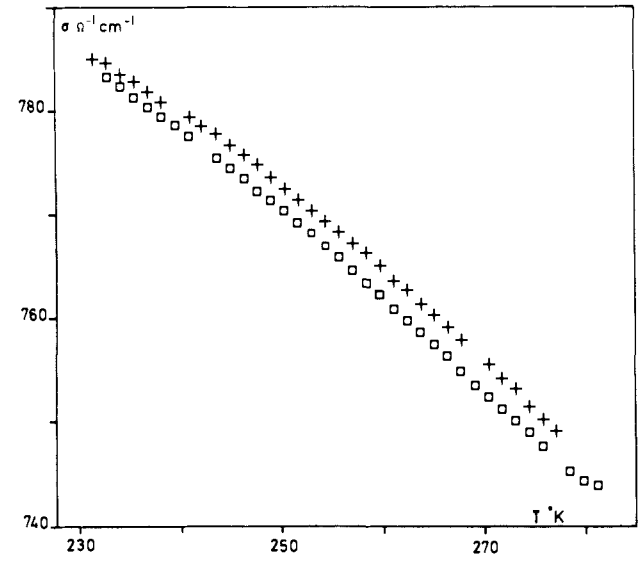

Figure 8. Conductivity vs. temperature for a crystal of $TTF[Pd(dmit)_2]_2$ between 300 and 240 K, measured on cooling (+) and subsequent warming (□).

compound is maintained on cycling throughout the temperature range of 300–240 K, i.e., *above* the transition temperature of 220 K. Crystals that have been once cooled to temperatures lower than 220 K were observed to retain their semiconducting behavior after storage at room temperature for periods up to 12 days.

Such a behavior is indicative of a structural phase transition at ca. 220 K. This observation is confirmed by a preliminary X-ray diffraction study which indicates the existence of three different phases (α, β, and γ). The α phase refers to a crystal which has never been cooled; it corresponds to the "metallic" part of the

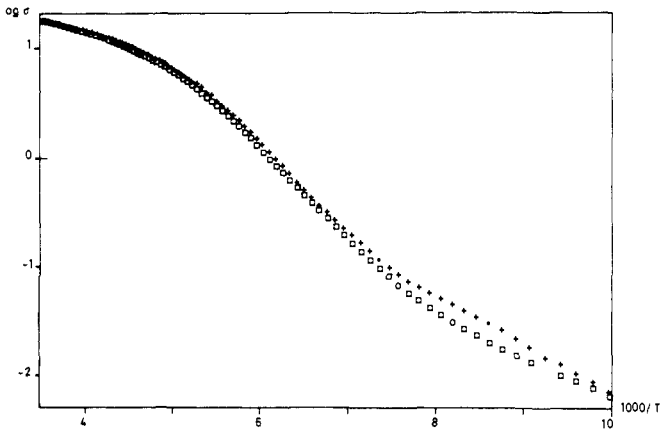

Figure 9. log conductivity vs. inverse of temperature for a crystal of $TTF[Pt(dmit)_2]_3$ between 300 and 100 K.

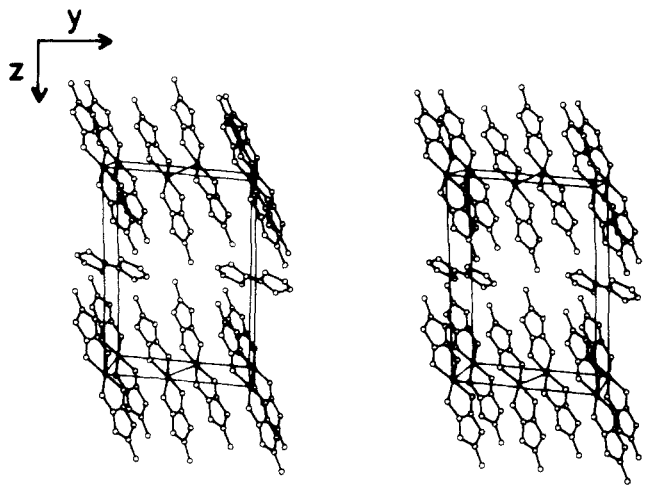

Figure 10. Stereoscopic drawing of the unit cell of $TTF[Pt(dmit)_2]_3$ viewed along a direction close to [100].

conductivity curve. This α phase (a = 46.81 (1) Å, b = 3.617 (2) Å, c = 23.083 (6) Å and β = 119.67° at 293 K) is isomorphous with the analogous nickel derivative. When the crystal is cooled, a phase transition is observed around 220 K, leading to a β phase (a = 46.67 (3) Å, b = 3.556 (2) Å, c = 22.92 (2) Å, and β = 119.88 (6)° at 120 K). When warmed back to room temperature, the β phase undergoes another transition at a temperature of ca. 230 K. A comparison of the intensities of the reflections used to follow the phase transition indicates that the γ pahse thus obtained, through isomorphous (a = 46.80 (1) Å, b = 3.615 (1) Å, c = 23.104 (6) Å, and β = 119.49 (2)° at 293 K), is structurally different from the α phase. A full detailed study of these different phases and transitions is under progress and will be reported elsewhere.

$TTF[Pt(dmit)_2]_3$. The room-temperature conductivity of this compound, measured along the needle axis ([1$\bar{1}$0]) is 20 Ω^{-1} cm^{-1}. Unlike the nickel and palladium derivatives, the crystals of the platinum compound are semiconductors throughout the entire range of temperatures investigated (300–100 K) (Figure 9). In the high-temperature range (300–200 K), the activation energy is very low (0.03–0.05 eV) and then increases (up to 0.2 eV) at lower temperatures.

The unit cell contains one TTF molecule, one *monomer* $Pt(dmit)_2$ molecule, and two $Pt(dmit)_2$ molecules connected by a Pt–Pt bond, thus forming a *dimer*. Within a dimer, the Pt–Pt bond length is 2.935 Å. These $[Pt(dmit)_2]_2$ dimers resemble closely the $[PtS_4C_4H_4]_2$ dimer units previously found in the crystal structure of the neutral $PtS_4C_4H_4$ complex.[32] The Pt–Pt distance

(32) Browall, K. W.; Bursh, T.; Interrante, L. V.; Kasper, J. S. *Inorg. Chem.* **1972**, *11*, 1800–1806.

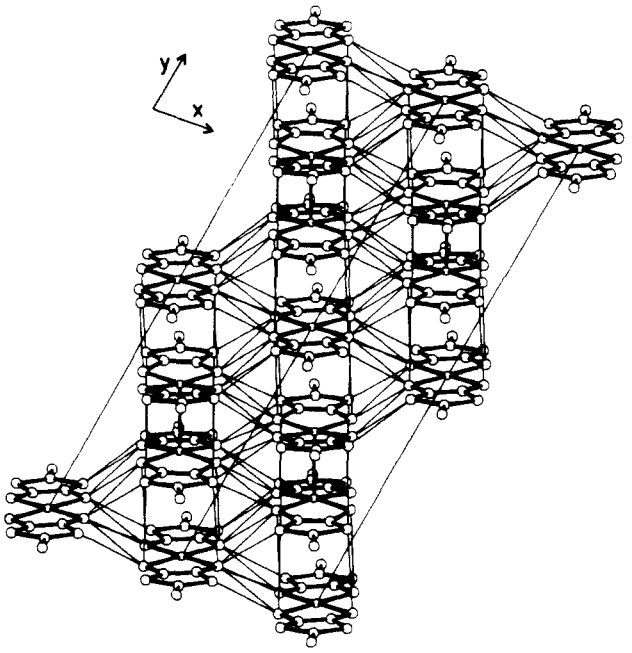

Figure 11. $TTF[Pt(dmit)_2]_3$. Parallel view of a layer containing stacks of $Pt(dmit)_2$ units. Within a stack, monomers and dimers alternate along [1$\bar{1}$0]. For the sake of clarity, the (001) plane is tilted out of the projection plane by 18° around an axis perpendicular to [1$\bar{1}$0]. Thin lines indicate S···S distances shorter than 3.70 Å.

Table VIII. $TTF[Pt(dmit)_2]_3$—Intermolecular S...S Distances (Å) Shorter than 3.70 Å. Estimated Standard Deviations Are 0.02 Å. Lower-Case Letters Refer to the Transformations (a) 1 + x,y,z; (b) $x-1,y,z$; (c) $-x,-y,-z$; (d) $-1-x,-y,-z$; (e) $-x,1-y,-z$; and (f) $-1-x,1-y,-z$

Intermolecular S...S Separations within a Stack			
S(1)...S(12)	3.65	S(1)...S(13c)	3.66
S(2)...S(11)	3.63	S(2)...S(14c)	3.63
S(6)...S(11f)	3.23	S(7)...S(12f)	3.23
S(8)...S(13f)	3.66	S(9)...S(14f)	3.63
Intermolecular S...S Separations between $Pt(dmit)_2$ Units of Adjacent Stacks			
S(1)...S(1d)	3.52	S(1)...S(2b)	3.52
S(1)...S(12d)	3.64	S(1)...S(14d)	3.60
S(2)...S(3a)	3.65	S(2)...S(6a)	3.51
S(2)...S(12a)	3.56	S(4)...S(6a)	3.53
S(4)...S(8a)	3.57	S(6)...S(7b)	3.54
S(6)...S(11b)	3.51	S(7)...S(8a)	3.64
S(7)...S(11e)	3.47	S(7)...S(13e)	3.51
S(11)...S(11e)	3.47	S(11)...S(12a)	3.54
S(12)...S(13b)	3.45		
Intermolecular S...S Separation between Monomer and TTF Molecules			
S(5)...S(16b)	3.45		

in the case of this sterically less-encumbered dimer is 2.748 Å, significantly shorter than the Pt–Pt bond in the $[Pt(dmit)_2]_2$ dimer unit. The TTF unit and the $Pt(dmit)_2$ monomer are centrosymmetric. An inversion center lies in the middle of the Pt–Pt bond of the $[Pt(dmit)_2]_2$ dimer. The structure consists of alternate layers parallel to the (001) plane (Figure 10), one layer containing both $Pt(dmit)_2$ monomers and $[Pt(dmit)_2]_2$ dimers and the other layer containing the TTF molecules.

In the $Pt(dmit)_2$ layers, the monomers and dimers are stacked in columns parallel to the [1$\bar{1}$0] direction (Figure 11). Within a column, monomers and dimers alternate. The perpendicular to the mean molecular plane of the $Pt(dmit)_2$ monomers, as well as the Pt–Pt bond of the dimer, makes an angle of ca. 23° with respect to the [1$\bar{1}$0] direction.[25]

As in the case of $PtS_4C_4H_4$, the two $Pt(dmit)_2$ units of a dimer are distorted from planarity as evidenced by the deviations of the atoms from their least-squares plane[25] and by the dihedral angle

Table IX. Comparison of Bond Lengths (Å) in TTF Averaged over Assumed *mmm* Symmetry

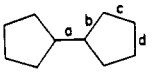

TTF bond length	TTF[a]	$(TTF)I_{0.71}$[b]	(TTF)(DETCNQ)[c]	(TTF)(TCNQ)[d]	$(TTF)(ClO_4)$[e]	$TTF[Ni(dmit)_2]_2$[f]	$TTF[Pt(dmit)_2]_3$[f]
a	1.349	1.350	1.367	1.372	1.404	1.35	1.40
b	1.757	1.732	1.750	1.745	1.713	1.735	1.73
c	1.730	1.721	1.720	1.739	1.725	1.735	1.77
d	1.314	1.336	1.323	1.326	1.306	1.27	1.30

[a] Cooper, W. F.; Kenny, N. C.; Edmonds, J. N.; Nagel, A.; Wudl, F.; Coppens, P. *J. Chem. Soc., Chem. Commun.* **1971**, 889–890. [b] Johnson, C. K.; Watson, C. R., Jr. *J. Chem. Phys.* **1976**, *64*, 2271–2286. [c] Schultz, A. J.; Stucky, G. D.; Craven, R.; Schaffman, M. J.; Salomon, M. B. *J. Am. Chem. Soc.* **1976**, *98*, 5191–5197. [d] Kistenmacher, T. J.; Phillips, T. E.; Cowan, D. O. *Acta Crystallogr., Sect. B* **1974**, *B30*, 763–768. [e] Yakushii, K.; Nishimura, S.; Sugano, T.; Kuroda, H. *Acta Crystallogr., Sect. B* **1980**, *B36*, 358–363. [f] This work.

of 11.2° between the two Pt(dmit) moieties in each $Pt(dmit)_2$ unit. This folding of the $Pt(dmit)_2$ units of the dimer results in increasing intermolecular–interatomic distances within a dimer when going away from the Pt atoms. A number of S···S contacts shorter than the sum of the corresponding van der Waals radii[31] (Table VIII and Figure 11) are observed: these interactions take place (i) within a stack and within a dimer as well as between dimers and monomers and (ii) between $Pt(dmit)_2$ units of either monomers or dimers belonging to adjacent stacks. Thus, these S···S interactions form a *two-dimensional* network in the (001) plane.

In the case of the TTF molecule, the only short intermolecular S···S contacts involve two TTF sulfur atoms and the terminal sulfur atoms of the monomeric $Pt(dmit)_2$ units. The three-dimensional character of this structure is less clear than in the case of the nickel derivative. As in the $Ni(dmit)_2$ case, there is no short S···S separations between the TTF molecules of a layer.

Discussion and Conclusions

The room-temperature conductivities of the $TTF[M(dmit)_2]_x$ compounds are among the highest yet observed for molecular solids in general and for transition-metal complexes in particular. In contrast to other bis(dithiolene) complexes, the $[M(dmit)_2]^{n-}$ system seems to be highly amenable to the formation of electronically conductive *two-dimensional* molecular networks. This was noted earlier in studies of both the structure and conductivity of its mixed-valence salts, $[Ni(dmit)_2]X_y$ (X = *n*-Bu_4N, y = 0.29;[18b] X = Et_4N, y = 0.5[19]) and of the donor–acceptor compound (BEDT-TTF)$[Ni(dmit)_2]$.[20b] These compounds are semiconductors with low activation energies and relatively high room-temperature conductivities. It is noteworthy that in these compounds, the anisotropy in the conductivities is quite low for two directions ($\sigma_a/\sigma_b/\sigma_c$ = 2:1:10^{-4} for $(n\text{-}Bu_4N)_{0.29}[Ni(dmit)_2]$;[18b] $\sigma_a/\sigma_b/\sigma_c$ = 1:50:8 for $(Et_4N)_{0.5}[Ni(dmit)_2]$;[19] σ_b/σ_c = 3.2 for (BEDT-TTF)$[Ni(dmit)_2]$[20b]). These experimental results suggest the existence of a structure–electrical properties relationship in such compounds; i.e., the dimensionality of the S···S interaction network is effectively related to the anisotropy in the conductivities.

The tendency of the $[M(dmit)_2]^{n-}$ units to form two-dimensional networks may stem from a combination of non-bonding repulsive interactions leading to a slipped-stack arrangement and the extension of the frontier orbitals of the complex to the peripheral sulfur atoms of the molecular units, thus providing effective overlap between molecules in adjacent "stacks".[33]

In the case of the $TTF[Ni(dmit)_2]_2$ derivative, the two-dimensional networks appear to be effectively linked by TTF molecules so as to provide a molecular metal with more nearly three-dimensional electronic interactions. However, due to the size and shape of the crystals (extremely thin and narrow needles), the conductivity could be determined by the four-probe method only along the needle axis ([010] direction). Therefore, no "physical" proof is yet available of appreciable conductivity in all directions. In this respect, our inability to observe an EPR signal, which we attribute to an extreme broadening of the expected line, may be considered as an experimental indication of the 3D metallic nature of this compound.

In the context of other "donor–acceptor" compounds, the TTF-$M(dmit)_2$ system possesses all the structural and electronic features considered necessary for high conductivity.[34–36] such as overall molecular planarity, close and segregated stacking, extended π-electron systems with good overlap, and closely matched redox potentials for the donor and acceptor units (TTF, 0.33 V vs. SCE;[37] $Ni(dmit)_2$, ca. 0.2 V vs. SCE[18,22]). However, unlike most other compounds of this type, the strong tendency to form 1D chains has been effectively eliminated, thereby circumventing the usual problem of Peierls transitions in 1D metal systems. This is particularly obvious in the case of the $TTF[Ni(dmit)_2]_2$ derivative which, in addition to having a high room-temperature conductivity, exhibits a metallike conductivity temperature dependence down to at least 4 K and becomes a superconductor under pressure below 1.6 K.[30c] This behavior is unique among previous examples of π donor–acceptor compounds, all of which exhibit a peak in conductivity at temperatures well in excess of 4 K.[2–4,16] The suppression of the Peierls transition in this case is probably due to the extensive three-dimensional molecular connectivity in the crystal structure of this compound evidenced by the short S···S intermolecular contacts extending along all three directions in the solid.

Similar interstack interactions involving sulfur or selenium in certain other molecular metal systems have been previously noted and related to the high conductivity observed for these solids at low temperatures. For example, $(TMTSF)_2AsF_6$ has been characterized as a quasi-two-dimensional system involving "selenium clustering".[14a] Likewise, the structures of some $(BEDT\text{-}TTF)_2Y$ (Y = I_3^-, ReO_4^-, and BrO_4^-) superconducting salts have been described as forming a "two-dimensional corrugated sheet network".[15c,38] In fact, in the BEDT-TTF-based compounds, the structural results strongly suggest that the *intrastack* interactions are less important than the *interstack* interactions in determining the solid-state electronic properties.[13,15,38]

In this context, it is noteworthy that in the crystal structure of $TTF[Ni(dmit)_2]_2$, there are no intermolecular contacts shorter than the corresponding van der Waals separations within the $Ni(dmit)_2$ "stacks" along [010], whereas there are a number of short S···S contacts between molecules in adjacent stacks (Figure 6). Due to the staggered arrangement of $Ni(dmit)_2$ molecules in these adjacent stacks, these interstack interactions produce a two-dimensional network of short S···S contacts in the (100) plane of the structure. Likewise, the separations between the TTF units along [010] (3.65 Å) are well in excess of those typically observed in electrically conductive TTF derivatives (3.47–3.57 Å),[39] ef-

(33) Alvarez, S.; Vicente, R.; Hoffman, R. Personal communication.

(34) (a) Epstein, A. J.; Miller, J. S. *Prog. Inorg. Chem.* **1976**, *20*, 1–52. (b) Interrante, L.; Bray, J.; Hart, H., Jr.; Kasper, J.; Piacente, P. *Ann. N. Y. Acad. Sci. U.S.A.* **1978**, *313*, 407–416.

(35) (a) Wheland, R. C. *J. Am. Chem. Soc.* **1976**, *98*, 3926–3930. (b) Torrance, J. B. *Acc. Chem. Res.* **1979**, *12*, 79–83.

(36) Delhaes, P. *Mol. Cryst. Liq. Cryst.* **1983**, *96*, 229–262.

(37) Scott, B. A.; Kaufman, F. B.; Engler, E. M. *J. Am. Chem. Soc.* **1976**, *98*, 4342–4344.

(38) Williams, J. M.; Beno, M. A.; Wang, H. H.; Reed, P. E.; Azevedo, L. J.; Schriber, J. E. *Inorg. Chem.* **1984**, *23*, 1790–1792.

fectively eliminating from consideration direct TTF-TTF coupling as an important factor in determining the solid-state properties of this compound. On the other hand, several quite short S···S contacts involving these TTF units and the terminal sulfur atoms of the $Ni(dmit)_2$ molecules are observed, suggesting the possibility of nearly isotropic electronic interactions. In view of the electrical conductivity behavior observed for this system, this prospect appears to have been realized, apparently leading to the first effectively 3D molecular metal.

The compound, $TTF[Pd(dmit)_2]_2$, which is isomorphous with the nickel derivative, exhibits the highest room-temperature conductivity (750 Ω^{-1} cm^{-1}) of any of the $TTF[M(dmit)_2]_x$ compounds. However, this compound exhibits a metallike conductivity temperature dependence only at temperatures above ca. 220 K and undergoes a peculiar metal-to-semiconductor transition below this temperature which results in an irreversible change in the electrical properties of the crystal. Explanation of this behavior may be found in a temperature-dependent structural determination which is in progress; preliminary results indicate that these conductivity changes are associated with structural phase transition(s) which occur at about this same temperature.

In the last example studied, $TTF[Pt(dmit)_2]_3$, the stoichiometry is now different from that observed for the nickel and palladium derivatives. Also different are the conductivity behavior and the structural arrangement. The thermally activated conductivity observed for the platinum compound may arise from the alternate stacking of monomer and dimer molecules within the $Pt(dmit)_2$ stacks which results in a gap in the band structure at the Fermi level. Nevertheless, the room-temperature conductivity of this compound is surprisingly high (20 Ω^{-1} cm^{-1}) compared to what might be expected on the basis of such a stacking arrangement. This high conductivity is probably due to the interstack electronic coupling evidenced by the high degree of molecular connectivity in the (001) plane.

It might be anticipated that information on the degree of charge transfer between the donor and acceptor molecules be derived from comparison of bond lengths of TTF in the $TTF[M(dmit)_2]_x$ compounds and other TTF^{n+} compounds for which the charge state is known. Such a comparison is shown in Table IX. Unfortunately, no clear trends in bond variations can be observed within the limits of the uncertainties in the measurements. This is partly due to insufficient accuracy in the various structure determinations and also to the necessary averaging over idealized molecular geometry (*mmm* symmetry). A similar result has been obtained[18,19] in the comparison of bond lengths of the $Ni(dmit)_2$ entities in various $[Ni(dmit)_2]C_x$ mixed-valence salts.

The main conclusion of this work is that the strategy of using sulfur atoms on the periphery of the molecular unit as a means of extending the π-electron system and promoting interstack coupling may be effective in realizing the objective of a 3D molecular metal. The results obtained here suggest that the $TTF[M(dmit)_2]_x$ compounds, especially the nickel derivative, approach this objective much more closely than any previous examples of molecular metals.

It is also clear that the nature of the metal atom M plays an important role in determining the structural and physical properties of the $TTF[M(dmit)_2]_x$ compounds. The capacity of this system for structural modification through changes in the metal, the dmit ligand, and the donor molecule gives the promise of a rich variety of new compounds with interesting electrical properties including potentially new superconductors.

Acknowledgment. We are grateful to the NATO Scientific Affairs Division for the support of this work. We thank the Motorola Co., Toulouse, for supplying mounted circuits used for the conductivity measurements. Helpful discussion on crystallographic aspects of this work with J. Kasper and J. Galy is gratefully acknowledged. We thank J. M. Williams for carrying out radio frequency field penetration depth measurements. We also thank R. Kato and H. Kobayashi for communicating their results on DBTTF[$Ni(dmit)_2$] and BEDT-TTF[$Ni(dmit)_2$] prior to publication.

Supplementary Material Available: Design of the solution diffusion cell (Figure 12), stereoscopic drawing of the unit cell of $TTF[Ni(dmit)_2]_2$ (Figure 13), view of a $Pt(dmit)_2$ stack in $TTF[Pt(dmit)_2]_3$ (Figure 14), X-ray powder diagrams for $TTF[M(dmit)_2]_2$ (M = Ni and Pd) and $TTF[Pt(dmit)_2]_3$ (Tables X and XI), observed and calculated structure factors, final thermal parameters, and hydrogen atomic positional parameters, respectively, for $TTF[Ni(dmit)_2]_2$ (Tables XII–XIV) observed and calculated structure factors and final thermal parameters, respectively, for $TTF[Pt(dmit)_2]_3$ (Tables XV and XVI), and deviations of atoms from their least-squares plane for $TTF[Ni(dmit)_2]_2$ and for $TTF[Pt(dmit)_2]_3$ and dihedral angles (Table XVII) (30 pages). Ordering information is given on any current masthead page.

(39) (a) La Placa, S. J.; Corfield, R. W. R.; Thomas, R.; Scott, B. A. *Solid State Commun.* **1975**, *17*, 635–638. (b) Scott, B. A.; La Placa, S. J.; Torrance, J. B.; Silverman, B. D.; Welber, B. *Ann. N. Y. Acad. Sci. U.S.A.* **1978**, *313*, 369–376. (c) Kistenmacher, T. J.; Philips, T. E.; Cowan, D. O. *Ibid.* **1978**, *313*, 333–342. (d) Torrance, J. B.; Mayerle, J. J.; Lee, V. Y.; Bechgaard, K. *J. Am. Chem. Soc.* **1979**, *101*, 4747–4748.